Kinetics of crystallization in hard-sphere colloidal suspensions

Narendra M. Dixit and Charles F. Zukoski*
Department of Chemical Engineering, University of Illinois at Urbana-Champaign, 114 Roger Adams Laboratory, 600 South Mathews Avenue, Urbana, Illinois 61801
(Received 27 February 2001; published 24 September 2001)

We propose a kinetic model for describing crystal nucleation kinetics in hard-sphere colloidal suspensions. The model captures the interplay between the enhanced thermodynamic driving force and the reduced particle diffusivity in determining crystal nucleation rates as the particle density is increased in hard-sphere suspensions. Model calculations of nucleation rates and crystal growth velocities agree quantitatively with experimental observations. The dependence of the critical cluster size on volume fraction that emerges differs qualitatively from predictions of classical theories allowing for an experimental validation of the mechanism of crystal nucleation in colloidal suspensions.

DOI: 10.1103/PhysRevE.64.041604 PACS number(s): 64.60.Qb

I. INTRODUCTION

Promising technological and scientific advances, such as the manufacture of photonic band gap materials and the determination of protein structures through x-ray crystallography, hinge on our ability to control colloidal crystallization [1,2]. Ongoing efforts to establish crystallization protocols have resulted in an understanding of the equilibrium phase behavior of large classes of colloidal suspensions, including hard spheres, proteins, globular macromolecules, and mixtures of colloids and polymers [3–10]. On the other hand, the kinetics associated with these phase transitions remains poorly understood. Classical nucleation theory is often invoked for predicting steady state nucleation rates during colloidal crystallization [11–15]. Comparisons between experimental results and model calculations show discrepancies that cannot be attributed easily to approximations in theory or uncertainties in experiment [11,16,17]. This is especially true of systems where particles have attractions. Even for hard spheres, where the phase diagram is well established, the rates of crystal nucleation and growth are difficult to predict [18]. As a result, colloidal crystals are often produced by highly empirical methods.

With the simplest of phase diagrams, suspensions of hard-sphere (HS) colloids are useful for studying the kinetics of colloidal crystallization. Here, only solid/fluid phase transitions are observed and the driving force for this ordering transition is controlled by a single parameter, the particle volume fraction, ϕ. The freezing boundary occurs at $\phi_s = 0.495$. For $\phi > \phi_s$, crystals with random stacking of hexagonal close-packed planes (rhcp) are seen in microgravity, whereas due to the inability to completely density match particles and the fluid, mixtures of face-centered-cubic (fcc) and rhcp arrangements occur under terrestrial conditions [19]. Due to the absence of particle interactions, except for an infinite repulsion at contact, crystallization in HS suspensions is entropic, with temperature playing no direct role in inducing phase changes. Cheng, Russel, and Chaikin demonstrated, however, that temperature gradients can induce crystallization indirectly, by altering the mechanical stability of the system, and allow for control of the crystallization process [20]. Crystallization can be suppressed by rapid increases in ϕ above ϕ_s [5]. A HS glass results at $\phi \approx 0.58$. At this volume fraction suspensions are observed to be nonergodic.

Nucleation rates, crystal growth velocities, and induction times have been measured for crystallization in HS suspensions [15,16,18,21–24]. At low volume fractions, $\phi \gtrsim \phi_s$, the kinetics of the phase transition is dictated predominantly by the thermodynamic driving force for crystallization, viz., the difference in the free energies of the solid and the fluid phases. Upon increasing ϕ above ϕ_s, the driving force increases and, accordingly, nucleation rates and growth velocities increase, and induction times decrease. At higher volume fractions, $\phi \approx 0.58$, hydrodynamic effects begin to dominate. Due to crowding, the diffusivity of the particles in suspension decreases. In this volume fraction regime, the rate of particle reorganization is a stronger function of volume fraction than the thermodynamic driving force. As a result, nucleation rates and growth velocities decrease, and induction times increase with increasing ϕ. These effects produce a maximum in the nucleation rate at $\phi \approx 0.56$.

Recently, with the particular aim of quantifying this competition between the thermodynamic and hydrodynamic effects, Russel adapted classical nucleation theory to describe crystal nucleation in HS suspensions [11]. In this approach, the nucleation rate is written as $I = A \exp(-\Delta G)$, where ΔG is the free energy barrier to crystal formation, and A is the prefactor characterized by the diffusivity of the particles in suspension. While classical theory is known to provide accurate expressions for ΔG, the prefactor A remains ambiguous [11]. Russel builds approximations for the long time and short time self-diffusivities of the particles in dense HS suspensions to determine A. Predictions of nucleation rates and growth velocities using these approximations agree qualitatively with experiments [11,16].

In a subsequent study, Ackerson and Schatzel argue that crystal formation and growth are not governed by the particle self-diffusivity but by the particle gradient diffusivity [12]. Their calculations suggest that the formation of a crystal

*Author to whom all correspondence should be addressed. Email address: czukoski@uiuc.edu

nucleus depletes the suspension of particles in the immediate vicinity of the crystal surface. A concentration gradient from the bulk suspension to the crystal surface is therefore established. Particles diffuse down this concentration gradient and are incorporated onto the crystal surface during nucleation and growth. The rates of these processes are controlled by the particle gradient diffusivity as opposed to the self-diffusivity. By incorporating these ideas in their adaptation of the classical theory, they find qualitative agreement between their predictions and experimental measurements of crystal growth rates. These studies and others [15,24] demonstrate that classical nucleation theory can predict nucleation rates during colloidal crystallization.

In making these predictions, the classical approach buries much of the kinetics of crystal nucleation in equilibrium thermodynamics. Indeed, in this lies the beauty of the classical approach. Nucleation, however, is an inherently kinetic phenomenon. Crystals do not appear spontaneously but are formed from particle aggregation and dissociation processes. We are interested ultimately in understanding the process by which crystals nucleate and grow, as this is important for interpreting light scattering data that determine induction times and crystal growth velocities used for characterizing nucleation kinetics. For this purpose, we are interested in developing a purely kinetic approach to describing colloidal crystallization.

In our previous work [25], the kinetic nucleation model proposed by Narasimhan and Ruckenstein [26] is adapted for systems where particles experience short-ranged attractions. In this approach, independent calculations of the rates of the aggregation and dissociation processes lead to predictions of nucleation rates and crystal growth velocities. The model captures much of the underlying physics of crystal nucleation but fails dramatically in quantitative comparisons with experimental data. This may be attributed to a series of assumptions made in the model that determine how strongly particles are bound to crystal surfaces. A second failure of the model as currently developed is that it cannot predict nucleation rates in purely repulsive systems, e.g., electrostatically stabilized or hard-sphere systems, where the ordering transition results from an increase in particle entropy in the crystalline phase over that in the fluid phase.

In this paper, we extend this kinetic model to the case of hard spheres. For this we note that although two isolated HS particles experience only volume exclusion interactions, when they are near each other in a dense suspension they experience a net attraction induced by local ordering, as indicated by the strong peak in the radial distribution function, $g(r)$, at contact [27]. We assume that this attraction drives crystallization in HS suspensions in a manner identical to that in attractive systems. This allows the extension of the current description of crystal nucleation to HS suspensions. Accurate quantitative predictions of nucleation rates, however, require a more sophisticated description of the crystal structure. Two terms of critical significance are involved: One is the number of nearest neighbors of particles on a crystal surface. The number of nearest neighbors determines the strength of the bonds holding the particles on the crystal surface. In the limit of infinitely large crystals, this number is set from estimates of the solid/fluid surface tension for HS systems. In the other limit where only two particles constitute a crystal nucleus, the number of nearest neighbors is set by assuming that particles in such a crystal have the same number of nearest neighbors as particles in the bulk fluid. How the number of nearest neighbors varies between these limits is not known. Approximating this size dependence introduces an adjustable parameter in our model. A second term of significance is the particle volume fraction in the depletion zone just outside the crystal surface. This must be below that in the bulk if there is to be a diffusional flux to the surface, as has been hypothesized by Ackerson and Schatzel [12]. Again, the equilibrium value is determined by requiring that infinitely large crystals do not grow or shrink. However, the dependence of this surface packing fraction on the bulk volume fraction remains unknown. We develop an approximation for this variation, which introduces a second nonequilibrium parameter in our model. We show that these two parameters can be chosen by fitting crystal growth rate data, and that once chosen, they predict nucleation rates well. In addition, we show that these parameters can be linked to the size and volume fraction dependence of the crystal/fluid surface tension—parameters commonly used for adjusting classical nucleation rate models to fit experimental data.

The paper is organized as follows. Below, in Sec. II, we briefly outline the equilibrium thermodynamics of HS suspensions. In Sec. III, we present a description of the crystal structure adopted in our model. In Sec. IV, we describe our method for calculating the aggregation and dissociation rates, leading to calculations of steady state nucleation rates and growth velocities. In Sec. V, we present calculations of nucleation rates and growth velocities and compare them with experimental results. In Sec. VI, we draw conclusions.

II. EQUILIBRIUM THERMODYNAMICS

A description of the equilibrium thermodynamics of HS suspensions is largely derived from computer simulations. The osmotic pressure of the fluid phase, P_f, is well approximated by the Carnahan–Starling equation of state [28]

$$\frac{4\pi a^3 P_f}{3\phi kT} = \frac{1+\phi+\phi^2-\phi^3}{(1-\phi)^3}, \tag{1}$$

where a is the radius of the colloidal particles in suspension, ϕ their volume fraction, and kT the product of the Boltzmann constant and the absolute temperature. An equation of state for the solid phase determined from computer simulations for a fcc crystal is given by [29]

$$\frac{4\pi a^3 P_s}{3\phi_{\text{xtal}} kT} = \frac{2.17}{0.738-\phi_{\text{xtal}}}, \tag{2}$$

where ϕ_{xtal} is the packing fraction in the solid phase. Given an equation of state, the chemical potential of the corresponding phase is determined as [11,12]

$$\frac{\mu}{kT} = \int \left(\frac{4\pi a^3 P}{3\phi kT} - 1\right)\frac{d\phi}{\phi} + \frac{4\pi a^3 P}{3\phi kT} + C, \tag{3}$$

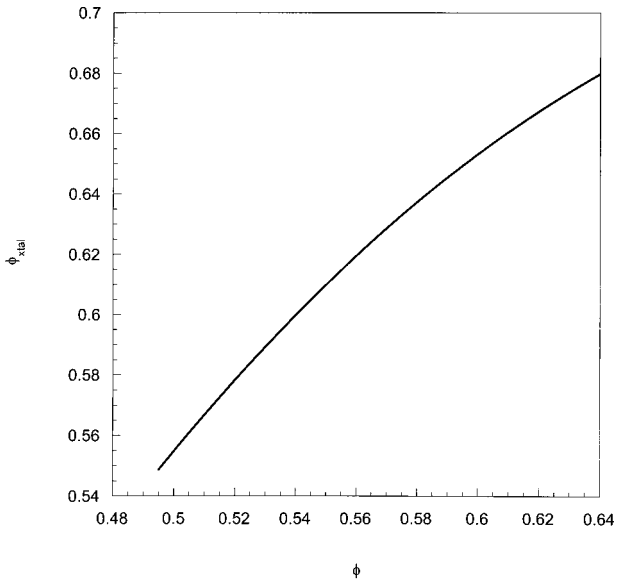

FIG. 1. Crystal packing fraction determined via Eq. (4) as a function of the volume fraction in the fluid phase.

where C is an arbitrary constant.

At equilibrium, the pressures and the chemical potentials of the solid and the fluid phases must be equal. This provides two equations for determining the volume fractions of the coexisting solid and fluid phases. At equilibrium, these volume fractions are 0.55 and 0.495, respectively. The fluid phase volume fraction at equilibrium sets the solubility boundary, $\phi_s = 0.495$, marking the onset of crystallization.

In a suspension of volume fraction $\phi > \phi_s$, crystals of volume fraction ϕ_{xtal} are formed. While $\phi_{\mathrm{xtal}} > \phi$ initially, the crystals eventually relax to the equilibrium volume fraction of 0.55 for $\phi_s < \phi < 0.55$, or ϕ for $\phi > 0.55$, as has been suggested by the work of Ackerson and Schatzel [12] and Palberg [15]. In the ensuing discussion, we are interested in knowing the volume fraction ϕ_{xtal} of a growing crystal, away from equilibrium. As an approximation, we determine ϕ_{xtal} from the condition of mechanical equilibrium, by equating the pressures in the solid and the fluid phases. This yields

$$\phi_{\mathrm{xtal}} = \frac{0.738}{1 + \dfrac{2.17(1-\phi)^3}{(1+\phi+\phi^2-\phi^3)\phi}}. \tag{4}$$

The resulting dependence of ϕ_{xtal} on ϕ is shown in Fig. 1. Experimental evidence of this approximation is provided by Harland and van Megen [24] who estimate ϕ_{xtal} and ϕ as crystallization progresses. They find that their data, at short times and initial volume fractions, $\phi > 0.55$, are captured well by Eq. (4). Note that for all $\phi > \phi_s$, $\phi_{\mathrm{xtal}} > \phi$. Therefore, as crystals nucleate, the average volume fraction in the fluid decreases below ϕ. In the coexistence region, i.e., $\phi_s < \phi < 0.55$, as time proceeds, ϕ approaches ϕ_s and ϕ_{xtal} approaches 0.55. Mass conservation then determines the fraction of the initial suspension converted to crystals. Outside the coexistence region, i.e., $\phi > 0.55$, where 100% conversion from fluid to crystal is observed [16], as time proceeds, crystals expand from ϕ_{xtal} to ϕ, and the fluid phase disappears. In the ensuing discussion, these ripening processes are assumed to occur over time scales much larger than the time scale for crystal nucleation and are therefore neglected. Crystals at packing fractions ϕ_{xtal} given by Eq. (4) are assumed to nucleate in background suspensions of volume fractions ϕ which do not vary with time.

III. CRYSTAL STRUCTURE

Classical theories employ a continuum description of crystal nuclei, with a sharp interface separating the crystals from the surrounding fluid. Such a description is adequate for determining the energetics of crystal formation, from which nucleation rates and growth velocities can be predicted. In the kinetic model presented here, accurate determination of the aggregation and dissociation rates of particles onto and from a crystal surface is crucial for accurate predictions of nucleation rates and requires a more detailed description of the crystal structure.

The crystal structure employed in our calculations is shown in Fig. 2. A crystal of radius R, consisting of uniformly distributed particles of radii a, is assumed to have a crystalline core of radius R-a at a volume fraction ϕ_{xtal}, determined from Eq. (4). This core is surrounded by a liquidlike surface layer of thickness a, at a packing fraction ϕ_R. The volume fraction of particles in the suspension rises from ϕ_R at the crystal surface to ϕ in the bulk suspension at large distances from the crystal.

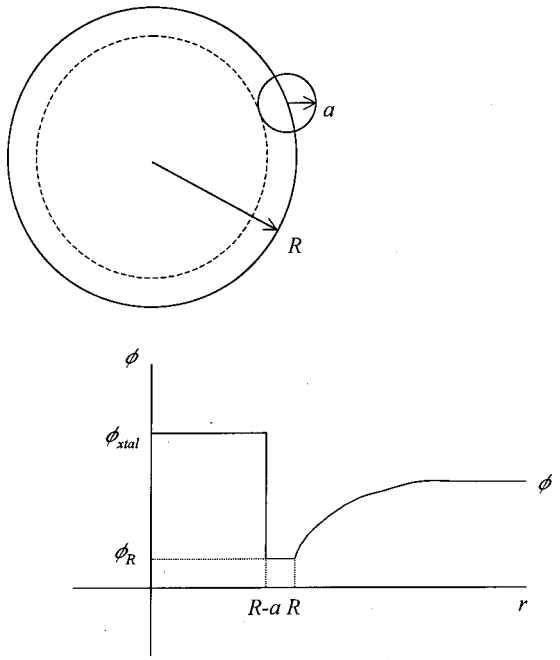

FIG. 2. The crystal structure assumed in our model consisting of a dense crystalline core of radius R-a at a packing fraction ϕ_{xtal} surrounded by a rare surface layer of thickness a (equal to the radius of a single particle) at a packing fraction ϕ_R. The volume fraction in the fluid phase rises from ϕ_R at the crystal surface to the bulk volume fraction, ϕ, at large distances from the crystal.

Since $\phi_{\text{xtal}} > \phi$, a depletion zone is formed adjacent to the crystal surface. As a consequence, we expect that the packing fraction in the fluid in the depletion zone to be smaller than ϕ (i.e., $\phi_R < \phi$). This results in a diffusional flux of particles from the bulk suspension to the crystal surface. Since ϕ_{xtal} varies with ϕ, we postulate that ϕ_R varies with ϕ as well. When $\phi = \phi_s = 0.495$, i.e., at the solubility point, we write $\phi_R = \phi_{\text{RS}}$. As discussed below, we determine ϕ_{RS} by requiring that at the solubility point no stable clusters can be formed. When $\phi = \phi_{\text{rcp}} = 0.64$, i.e., when the bulk fluid is randomly close packed, compaction of a certain region in the bulk fluid to a crystalline structure with a packing fraction ϕ_{xtal} is prevented due to the jamming of the particles. At this point, a distinct depletion zone ceases to exist, so that, $\phi_R = \phi = \phi_{\text{rcp}} = 0.64$. For $\phi_s < \phi < \phi_{\text{rcp}}$, the dependence of ϕ_R on ϕ is assumed to be of the form

$$\phi_R = \phi_{\text{RS}} = (\phi_{\text{rcp}} - \phi_{\text{RS}}) \exp\left\{ \frac{\xi(\phi - \phi_{\text{rcp}})}{(\phi - \phi_s)} \right\}, \tag{5}$$

where ξ is an adjustable parameter chosen as discussed below. In this description, we assume ϕ_R to be independent of R. We note that the functional form of Eq. (5) is arbitrary. We chose this function as a smooth interpolation between the two known limits with a single adjustable parameter ξ.

Particles within the crystalline core are assumed to have $C_{\text{xtal}} = 12$ nearest neighbors. In the surface layer, particles have C_s nearest neighbors, whereas in the bulk fluid they have C_f nearest neighbors. From geometric considerations the variation of C_s with R can be determined for a crystal with a densely packed surface layer [30]. For crystals with the rare surface layers assumed here, this variation is more complex and is assumed to be of the form

$$C_s(R) = C_f + (C_{s\infty} - C_f)\left(1 - \exp\left\{ \frac{\zeta(R_{\min} - R)}{2a} \right\} \right), \tag{6}$$

where ζ is an adjustable parameter chosen as discussed below. Here, $C_{s\infty}$ is the number of nearest neighbors of a particle on the surface of an infinitely large crystal and is determined from considerations of the solid/fluid surface tension. $R_{\min}$ is the size of a crystal containing two particles. A particle in such a crystal is assumed to have the same number of nearest neighbors as a particle in the bulk fluid. (Single particle crystals are not allowed in this model since dissociation of particles from such crystals is meaningless.) Thus, when $R = R_{\min}, C_s = C_f$. By assuming such a crystal to be close packed ($\phi_{\text{xtal}} = \phi_{\text{cp}} = 0.74$), we find

$$R_{\min} = a(2/\phi_{\text{cp}})^{1/3}, \tag{7}$$

which sets the minimum size of a crystal in suspension. That observed crystals are mixtures of rhcp and fcc structures suggests that crystal nuclei will not be spherical and their surfaces will not be smooth. More recent observations indicate that nuclei resemble ellipsoidal shapes more than spherical [31]. However, the exact shape of the nuclei is complicated and we proceed with the spherical approximation for the present calculations. Again, we note that the form of Eq. (6) is chosen to interpolate smoothly between two known limits with a single adjustable parameter.

IV. CRYSTAL NUCLEATION AND GROWTH

In a HS suspension of particle volume fraction $\phi > \phi_s$, crystals nucleate at a steady state nucleation rate, I, that is a function of the rate at which particles aggregate onto the crystal surface, β, and the rate at which particles leave the crystal surface, α. α and β have dependencies on the crystal size such that small crystals shrink and large ones grow. The critical cluster size is defined at each ϕ as that size at which $\alpha = \beta$. The rate of formation of clusters of the critical size gives the nucleation rate, I.

To determine α and β, and hence I, we consider a crystal nucleus of radius R in a suspension of volume fraction ϕ. Let the crystal nucleus consist of N particles, N_s of which lie in a surface layer of thickness a. Only some portion of each of these N_s particles will lie entirely within the crystal. On an average, the volume of this portion is given by [25]

$$V_s = \frac{2}{3}\pi a^3 \left[1 - \frac{a}{2R} \right]. \tag{8}$$

Since the surface layer has a packing fraction ϕ_R, N_s varies with R as

$$N_s = 2\left(\frac{R}{a} \right)^3 \phi_R \frac{[1 - (1 - a/R)^3]}{[1 - a/2R]}. \tag{9}$$

Two isolated HS particles in suspension experience only volume exclusion interactions. However, the presence of other particles in a suspension induces local ordering of these particles, characterized by the pair distribution function, $g(r, \phi)$, where r is the center-to-center separation between the particles. This ordering gives rise to an interaction between these particles other than the infinite repulsion at contact, and is characterized by a potential of mean force, defined as [27]

$$W(r, \phi) = -kT \ln g(r, \phi). \tag{10}$$

The prominent primary maximum in $g(r, \phi)$ and the corresponding minimum in $W(r, \phi)$ at $r = 2a$ for a dense suspension, i.e., $\phi \approx 0.5$, indicates the propensity of two particles in such a suspension to stay in contact rather than separated. This may be treated as a net attraction between two particles when they are sufficiently close to each other ($r < 3a$).

On the surface of a crystal, a particle is in contact with C_s other particles. If we assume that the potential of mean force is pair-wise additive, the surface particle will have an attraction energy of $C_s W(2a, \phi_R)$ binding it to the crystal. In the fluid just surrounding the crystal surface, a particle has C_f nearest neighbors. Therefore, the depth of the potential well in which a surface particle may be assumed to reside will be

$$\Phi = (C_s - C_f) W(2a, \phi_R) = -kT(C_s - C_f) \ln\{g(2a, \phi_R)\}. \tag{11}$$

The motion of the particle in this potential well is described by the Smoluchowski equation [25,26]. Solving this equation we obtain the mean residence time of the particle in this well, T_0. The extent of the potential well is assumed to be a, so that a particle on the surface escapes the well upon traversing an outward radial distance a. Then, the average dissociation rate at which particles escape the surface layer is calculated as $\alpha = N_s/T_0$. Following Dixit and Zukoski [25], we obtain

$$\alpha = \frac{6D_o\omega\phi_R R}{a^3[g(2a,\phi_R)]^{C_s - C_f}} \frac{[1-(1-a/R)^3]}{[1-a/2R]} \frac{[1+a/R]^2}{[(1+a/R)^3-1]}, \tag{12}$$

which for $R \gg a$ simplifies to $\alpha = 6D_o\omega\phi_R R/a^3[g(2a,\phi_R)]^{Cs-Cf}$. Here $\omega = 0.2$ is the approximate near field hydrodynamic contribution, reducing the diffusivity of the particles on the surface from D_o, the Stokes–Einstein diffusivity of the single particles in suspension [25]. The contact value of the pair distribution function is related to the osmotic pressure in the fluid phase as $4\pi a^3 P_f/3\phi kT = 1 + 4\phi g(2a,\phi)$ [27]. Combined with the Carnahan–Starling equation of state [Eq. (1)], this yields

$$g(2a,\phi) = \frac{1-\phi/2}{(1-\phi)^3}. \tag{13}$$

The aggregation rate of particles, β, occurring via gradient diffusion, is given by a solution of the standard diffusion equation. Following Dixit and Zukoski [25], we find that for a crystal of radius R in a suspension of bulk volume fraction ϕ

$$\beta = \frac{3R}{a^3}\left(1 + \frac{a}{R}\right)\int_{\phi_R}^{\phi} D(\phi')\,d\phi'. \tag{14}$$

Here, $D(\phi)$ is the gradient diffusivity of the particles in suspension and is given by

$$D(\phi) = D_o K(\phi)\frac{\partial}{\partial\phi}(\phi Z(\phi)), \tag{15}$$

where $K(\phi)$ is the hydrodynamic contribution to the diffusivity and is approximated as

$$K(\phi) = (1-\phi)^{6.55} \tag{16}$$

for hard spheres [32]. The thermodynamic contribution, $\partial(\phi Z(\phi))/\partial\phi$, is evaluated using the Carnahan–Starling equation of state, where $Z(\phi) = 4\pi a^3 P_f/3\phi kT$.

The calculation of α and β from the above expressions requires knowledge of two parameters, $C_{s\infty} - C_f$ and ϕ_{RS}, and links back to the crystal structure described in Sec. III. To determine $C_{s\infty}$, we note that the energy of formation of a crystal of radius R, containing a total of N particles, is approximately given by

$$U = (1/2)[-(N-N_s)C_{\mathrm{xtal}}kT\ln g(2a,\phi_{\mathrm{xtal}}) - N_s C_s kT\ln g(2a,\phi_R) + NC_f kT\ln g(2a,\phi)]. \tag{17}$$

Rearranging to group terms linear in N_s results in

$$U = -(1/2)N[C_{\mathrm{xtal}}kT\ln g(2a,\phi_{\mathrm{xtal}}) - C_f kT\ln g(2a,\phi)] + (1/2)N_s[C_{\mathrm{xtal}}kT\ln g(2a,\phi_{\mathrm{xtal}}) - C_s kT\ln g(2a,\phi_R)], \tag{18}$$

where we follow Narasimhan and Ruckenstein [26] to define the second term in Eq. (18) to correspond to the surface energy contribution in the formation of a crystal. When $R \gg a$, this is written as $4\pi R^2\gamma$, where γ is the solid/fluid surface tension. Thus when $\phi \approx \phi_s$ and $\phi_R \approx \phi_{\mathrm{RS}}$, we find $N_s \approx 6R^2\phi_{\mathrm{RS}}/a^2$ and $C_s \approx C_{s\infty}$ yielding

$$\frac{\gamma a^2}{kT} = \frac{3\phi_{\mathrm{RS}}}{4\pi}[C_{\mathrm{xtal}}\ln g(2a,\phi_{\mathrm{xtal}}) - C_{s\infty}\ln g(2a,\phi_{\mathrm{RS}})]. \tag{19}$$

From studies in the literature, for example, the work of Marr and Gast [33], a reasonable estimate for the surface energy of a HS crystal is given by $\gamma a^2/kT = 0.16$. Assuming $C_{\mathrm{xtal}} = 12$, and knowing $g(2a,\phi)$ for all ϕ, Eq. (19) provides one equation linking ϕ_{RS} and $C_{s\infty}$.

A second condition for determining the unknown equilibrium parameters can be obtained by noting that under the same conditions, i.e., $\phi = \phi_s$ and $\phi_R = \phi_{\mathrm{RS}}$, the critical cluster size diverges, so that, $\alpha = \beta$ as $R \to \infty$. This gives, from known expressions for α and β for $R \gg a$

$$\int_{\phi_{\mathrm{RS}}}^{\phi_s} \frac{D.(\phi')}{D_o}\,d\phi' = \frac{2\omega\phi_{\mathrm{RS}}}{[g(2a,\phi_{\mathrm{RS}})]^{C_{s\infty}-C_f}}. \tag{20}$$

Equation (20) links ϕ_{RS} and $C_{s\infty} - C_f$. C_f can be determined from simulations [34] or from an integral of $g(r,\phi)$, as has been done in the work of Chang and Sandler [35]. Knowing C_f, Eqs. (19) and (20) can be solved to find ϕ_{RS} and $C_{s\infty}$.

With both the parameters, ϕ_{RS} and $C_{s\infty} - C_f$, known, α and β can be calculated as functions of R and ϕ from Eqs. (5)–(7),(12)–(16). At any $\phi > \phi_s$, a critical cluster size, R^*, is defined as that size at which $\alpha = \beta$. Thus, R^* is obtained by equating Eqs. (12) and (14) and solving for R.

Assuming the background particle volume fraction to remain constant, a population balance yields the steady state nucleation rate as [25]

$$I = \frac{3\beta\phi}{8\pi a^3}\left(\frac{w''(N^*)}{\pi}\right)^{1/2}\exp(2w(N^*)), \tag{21}$$

where

$$w(N) = \int_0^N \frac{\beta-\alpha}{\beta+\alpha}\,dN \tag{22}$$

and $N=\phi_{\rm xtal}(R/a)^3$ is the number of particles in a crystal of size R. N^* is the number of particles in a crystal of the critical size, R^*, and $w''(N^*)$ is the second derivative of $w(N)$ with respect to N, evaluated at N^*.

The difference between α and β determines the growth velocity of a crystal. From a differential volume balance, we obtain for a crystal of size R in a suspension of volume fraction ϕ

$$\frac{dR}{dt}=\frac{(\beta-\alpha)\alpha^3}{3R^2\phi_R}. \tag{23}$$

Using these equations, we present calculations of nucleation rates and growth velocities and compare them with experimental observations in the next section.

V. CALCULATION OF NUCLEATION AND GROWTH RATES

We compare our model calculations with the experiments of Palberg [15] who studied the crystallization of HS particles of radii $a=435$ nm under conditions where the Stokes–Einstein diffusivity of the particles in suspension is $D_o=5.0\times10^{-9}$ cm^2/s. When the colloid volume fraction, ϕ, exceeds the solubility limit, $\phi_s=0.495$, the particles crystallize into structures with $C_{\rm xtal}=12$ nearest neighbors. In this range of volume fractions, following previous estimates [34,35], we let the number of nearest neighbors of particles in the bulk fluid be $C_f=9$ and assume that this does not vary with ϕ.

To determine nucleation rates, Eqs. (19) and (20) must be solved simultaneously to find $\phi_{\rm RS}$ and $C_{s\infty}$. The equations can be simplified by letting $\phi_{\rm RS}\approx\phi_s$ in Eq. (19) and noting that when $\phi=\phi_s=0.495$, $\phi_{\rm xtal}=0.55$, so that $\ln g(2a,\phi_{\rm xtal})\approx\ln g(2a,\phi_s)$. Then, solving Eq. (19) with $\gamma a^2/kT=0.2$, we find $C_{s\infty}=11$. With $C_{s\infty}-C_f=11-9=2$, solving Eq. (20) yields $\phi_{\rm RS}=0.486$, in agreement with our initial assumption that $\phi_{\rm RS}\approx\phi_s$.

Knowing these parameters, the dependence of the surface packing fraction, ϕ_R, on ϕ, and the dependence of the number of nearest neighbors, C_s, of a surface particle on the crystal size R can be determined from Eqs. (5) and (6), respectively. These dependencies are shown in Figs. 3 and 4 as functions of the parameters ξ and ζ. The choices of ξ and ζ are crucial to the quantitative capabilities of the nucleation rate model. The difference between ϕ and ϕ_R provides the requisite concentration gradient for the aggregation of particles from the bulk suspension onto a crystal surface and sets the magnitude of the aggregation rate. This gradient is small when $\phi\approx\phi_s$ and $\phi\approx\phi_{\rm rcp}$ and goes through a maximum at an intermediate ϕ. The parameter ξ determines the location of this maximum and, therefore, the location of the maximum in the nucleation rate. Similarly, C_s determines the magnitude of the potential well in which surface monomers lie and sets the magnitude of their dissociation rate. By varying ζ, the dissociation rate, the critical cluster size and, hence, the nucleation and growth rates can be varied quite sensitively. Here, we choose ξ and ζ to match the known growth rate data for hard-sphere crystals.

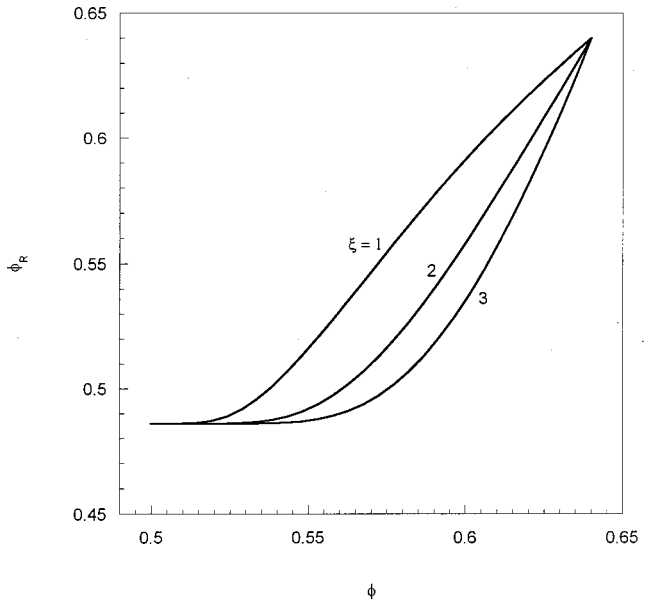

FIG. 3. The surface packing fraction calculated using Eq. (5) as a function of the bulk volume fraction for several values of the parameter ξ.

Using small angle light scattering and Bragg scattering, Palberg [15] measured crystal growth rates for the system discussed above for $\phi=0.535$ and these data are reproduced in Fig. 5. These data can be predicted using our model and require the integration of Eq. (23). This latter equation captures the growth of crystals bigger than the critical size, R^*, alone. Crystals of size R^* neither grow nor shrink, whereas crystals of size smaller than R^* are predicted to shrink. Hence, the use of Eq. (23) requires the assumption that a

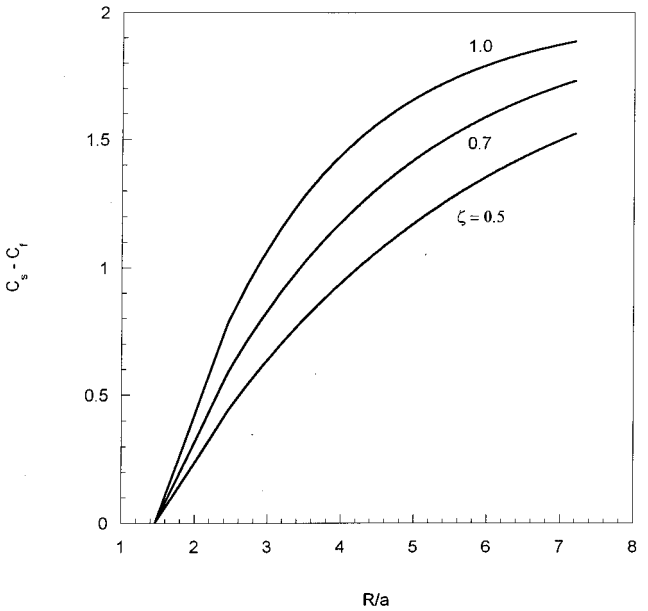

FIG. 4. The number of nearest neighbors of a particle on a crystal surface, C_s, in excess of that in the bulk fluid, C_f, calculated using Eq. (6) as a function of the crystal size R for several values of the parameter ζ.

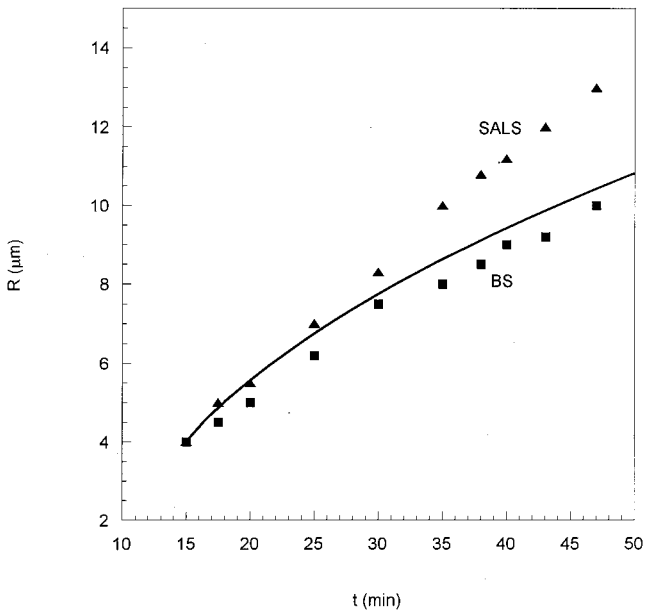

FIG. 5. Time evolution of the size of a growing crystal observed via small angle light scattering (triangles) and Bragg scattering (squares) under identical conditions (see Ref. [15]). The solid line is obtained by integrating Eq. (23) as described in the text with the parameters $\xi=2$ and $\zeta=0.7$.

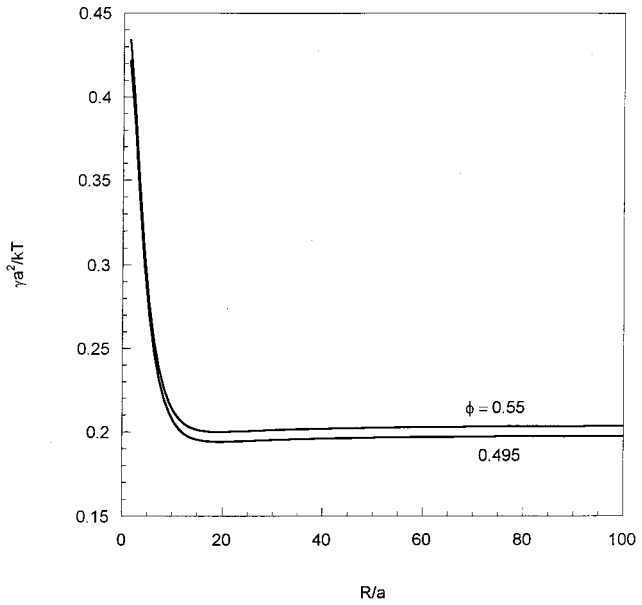

FIG. 6. Solid/fluid surface tension as a function of the crystal size calculated via Eq. (24) for two values of the bulk volume fraction.

concentration fluctuation produces a crystal of size bigger than R^* at some time t. Here, drawing from the experimental data, we assume that a crystal of radius $R=4\ \mu$m exists in the suspension at time $t=15$ min. The subsequent evolution of this crystal is predicted by integrating Eq. (23). This is shown in Fig. 5 for the values $\xi=2$ and $\zeta=0.7$ which, we find, provide the best agreement with the experimental data. We use these values for all further calculations.

The parameters ξ and ζ can be linked to the curvature and the volume fraction dependence of the solid/fluid surface tension. We note that the second term in Eq. (18) corresponds to the surface energy contribution to the formation of a crystal of size R in a suspension of volume fraction ϕ. Therefore, equating it to $4\pi R^2\gamma(R,\phi)$, we obtain

$$\frac{\gamma(R,\phi)a^2}{kT}=\frac{\phi_R R}{4\pi a}\frac{(1-(1-a/R)^3)}{(1-a/2R)}[C_{\rm xtal}\ln g(2a,\phi_{\rm xtal}) - C_s\ln g(2a,\phi_R)]. \quad (24)$$

Here, the parameter ξ determines the dependence of γ on ϕ, entering Eq. (24) via ϕ_R, and ζ determines the dependence of γ on R via C_s. For the above values of ξ and ζ, in Fig. 6 we show γ as a function of R for two different values of ϕ predicted by Eq. (24). In these calculations, we have assumed that $\ln g(2a,\phi_{\rm xtal})\approx\ln g(2a,\phi_R)$. The calculations suggest that in the range $\phi_s<\phi<0.55$, where Eq. (13) is known to predict $g(2a,\phi)$ accurately, γ is nearly independent of ϕ. The dependence on R, however, is more sensitive. As R increases above $R_{\rm min}$, γ decreases rapidly, passes through a weak minimum, and plateaus at very large values of R. These trends are in qualitative agreement with previous calculations [36–45]. The insensitivity of γ to ϕ is argued to be observed in systems where C_s is independent of ϕ [36], as is assumed in our model.

The dependence of γ on R is described using the simplified Tolman equation, $\gamma(R)=\gamma_\infty(1-2\delta_\infty/R)$, where γ_∞ is γ for the planar interface ($R\to\infty$) and $\delta_\infty(\ll R)$ is δ, the Tolman length, again for $R\to\infty$ [37]. Simplifying Eq. (24) to terms linear in a/R and comparing it with the Tolman equation, we find that $\delta_\infty\approx a/4$, in reasonable agreement with previous calculations [38–40]. The Tolman length δ for smaller R is predicted to have a strong dependence on R [40,41]. Depending on whether δ is positive or negative, γ is found to increase or decrease, respectively, upon increasing R. Thus, the nonmonotonic variation of γ with R predicted by Eq. (24) indicates that δ changes sign upon increasing R. Similar nonmonotonic variations in γ and corresponding changes in the sign of δ have been predicted in previous studies [41–43]. Further, we note that the work of Israelachvili [44] and Sinanoglu [45] suggests that over a broad range of droplet sizes, γ is independent of R, but begins to vary when R is on the order of the size of the particles constituting the fluid. In reasonable agreement, we find that the γ becomes independent of R (as suggested by the onset of the plateau in Fig. 6) when $R\approx 10a$.

Having set the values of the parameters ξ and ζ, α and β can be calculated for all R and ϕ. Shown in Fig. 7 are α and β as functions of R for $\phi=0.5$. For a fixed value of ϕ, $\alpha>\beta$ for small R, and vice versa for large R. Thus, small crystals shrink and large crystals grow. The critical cluster size R^* occurs when $\alpha=\beta$. At a fixed value of R, α decreases monotonically upon increasing ϕ as $g(2a,\phi_R)$ increases monotonically. On the other hand, β first increases and then decreases upon increasing ϕ. This behavior is governed by the difference between ϕ_R and ϕ, which goes

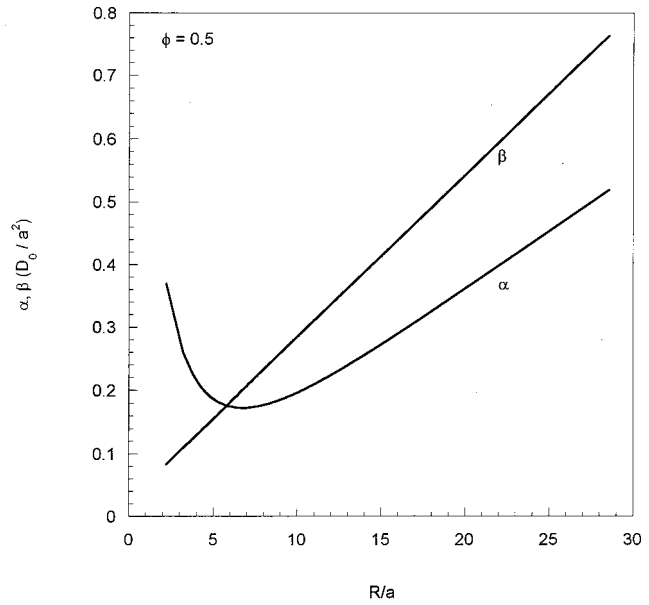

FIG. 7. Dissociation (α) and aggregation (β) rates calculated as functions of the crystal size at a suspension volume fraction ϕ of 0.5. The point of intersection of the two curves gives the critical cluster size R^* at that volume fraction.

through a maximum upon increasing ϕ (see Fig. 3). Thus, upon increasing ϕ above but close to ϕ_s, α decreases and β increases, resulting in a decrease in R^*. At much larger values of ϕ, while α continues to decrease, β begins to decrease as well. Here, β is a stronger function of ϕ than α and results in an increase in R^* with ϕ. R^* therefore goes through a minimum upon increasing ϕ. Shown in Fig. 8 are calculations of R^* as a function of ϕ. R^* diverges at $\phi=\phi_s$ and at $\phi=\phi_{\mathrm{rcp}}$, by construct, and passes through a minimum at $\phi\approx 0.56$.

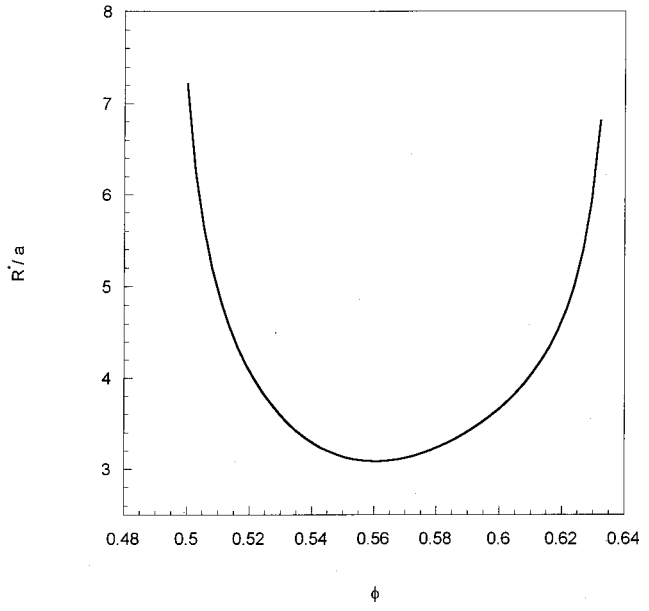

FIG. 8. Critical cluster size as a function of volume fraction.

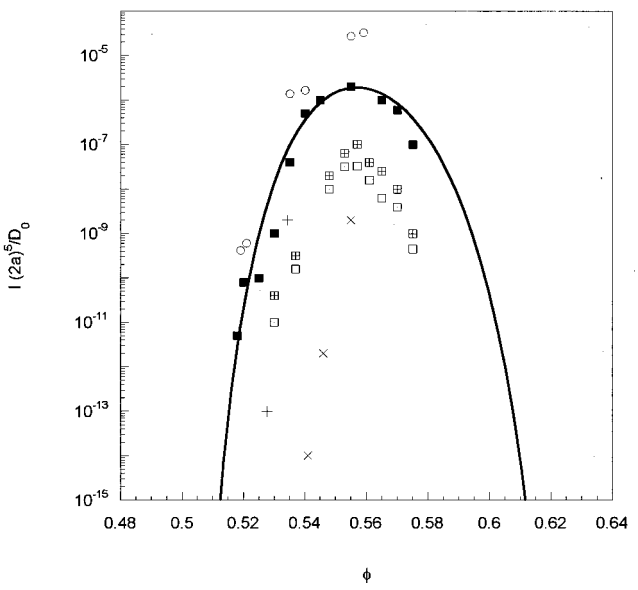

FIG. 9. Nucleation rate as a function of volume fraction calculated (solid line) via Eq. (21) and compared to the experimental estimates from Palberg (see Ref. [15]) (filled squares), Schatzel and Ackerson (see Ref. [16]) (circles), maximum (checkered squares) and average (dotted squares) nucleation rates from Harland and van Megen (see Ref. [24]), and from simulations of monodisperse (+) and polydisperse (×) hard sphere systems by Auer and Frenkel (see Ref. [46]).

In Fig. 9, we present calculations of nucleation rates, I, from Eq. (21). In accordance with classical theories, I is zero when $\phi=\phi_s$, and increases upon increasing ϕ due to the increasing thermodynamic driving force for crystallization. At larger ϕ, however, I is reduced due to hydrodynamic effects. A maximum occurs at $\phi\approx 0.56$. Shown in the same figure are nucleation rates determined via scattering experiments by Palberg [15]. Note that there are no adjustable parameters used in this figure. Excellent agreement is seen between the experimental results and model calculations. The model predicts the experimental nucleation rates accurately until $\phi\approx 0.56$. Beyond $\phi\approx 0.56$, the model tends to overpredict the experimental data. One reason for this may be attributed to the intervening glass transition, which occurs at $\phi\approx 0.58$. In the absence of a glass transition, as assumed in this model, particle jamming occurs at the random close packing volume fraction, $\phi_{\mathrm{rcp}}=0.64$. However, a glass transition forces jamming at $\phi\approx 0.58$, resulting in much lower nucleation rates in this volume fraction range than predicted.

Also shown in the same figure are nucleation rates estimated by Schatzel and Ackerson [16] and Harland and van Megen [24] from scattering experiments, and by Auer and Frenkel [46] from simulations. The discrepancy between the results of independent experiments and between experiments and simulations is glaring. Auer and Frenkel argue that the reason for the discrepancy lies in the interpretation of the experiments. Classical nucleation theory has been shown to capture the experimental nucleation rates, although with the surface tension, γ, as the adjustable parameter. Auer and

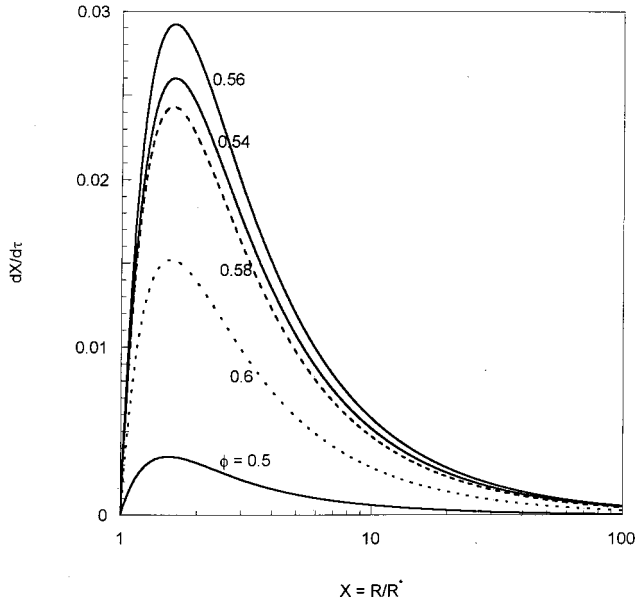

FIG. 10. Nondimensional growth rates calculated using Eq. (23) as functions of the reduced crystal size for several volume fractions.

Frenkel find that the values of γ obtained from such fits ($\gamma a^2/kT \approx 0.12$) are lower than those obtained from fits to their simulation data ($\gamma a^2/kT \approx 0.18$). However, more recent experiments involving the real space imaging of the nucleation of crystals of slightly charged spheres [31] have provided estimates of $\gamma(\gamma a^2/kT \approx 0.03)$ that are much lower than the estimates from fits using classical theory. The reported nucleation rate estimates from these experiments (e.g., $I \approx 1.0\,\mathrm{mm}^{-3}\,\mathrm{s}^{-1}$ at $\phi \approx 0.5$, which corresponds to $32Ia^5/D_o \approx 10^{-5}$ at $\phi_{\mathrm{eff}} \approx 0.56$) are comparable to the other experimental estimates. Thus, the discrepancy between the nucleation rates estimated from different experiments and simulations remains a matter of concern. More detailed real space experiments may resolve these differences.

Finally, we note that the growth rate predictions of Eq. (23) agree with the dynamical scaling of crystal growth observed experimentally. Schatzel and Ackerson [16] find that at long times, crystal growth follows the $R \sim t^{1/2}$ scaling when ϕ lies in the coexistence region, i.e., $\phi_s < \phi < 0.55$. (For $\phi > 0.55$, this scaling could not be unambiguously identified.) In our model, such a scaling emerges in the limit of large crystal sizes, $R \gg a$. Under these conditions, both α and β scale as $\sim R$. Then, Eq. (23) simplifies to $dR/dt \sim 1/R$, integrating which yields the $R \sim t^{1/2}$ scaling. Further, as shown in Fig. 5, rigorous integration of Eq. (23) captures the time evolution of growing crystals quantitatively. Ackerson and Shatzel [12] and Russel *et al.* [47] predict this scaling from their adaptations of the classical growth models. For a comparison with their predictions, we present in Fig. 10 dimensionless growth rates $dX/d\tau$ calculated using Eq. (23) as functions of X for several values of ϕ. Here, $X = R/R^*$ is the dimensionless crystal radius and $\tau = tD_o/(R^*)^2$ is the dimensionless time. $dX/d\tau$ is zero for $X = 1$ as at this point $\alpha = \beta$ for all ϕ. For $X > 1$, $dX/d\tau$ increases as X increases, reaches a maximum, and finally decays to zero asymptotically for large X. The maximum, occurring at $X \sim 2$, corresponds to the minimum in α [or, to be precise, the maximum in $(\beta - \alpha)/R^2$] as indicated in Fig. 7 which sets the magnitude of the growth rate in Eq. (23). The asymptotic decay is due to the $1/R$ dependence of the growth rate for $R \gg a$ as described above. This behavior is in excellent agreement with the calculations of Russel *et al.* [47] for $\phi < 0.55$. The maximum in their calculations, which also occurs at $X \sim 2$, is attributed to the effects of surface tension. For $\phi > 0.55$, the assumption of no surface tension in their model yields a size independent growth rate according to the classical Wilson–Frenkel growth law.

The model presented here thus captures quantitatively experimental observations of the kinetics of crystallization in HS suspensions. While doing so, we note that it employs a completely kinetic description of nucleation that differs significantly from classical theories. Models based on classical nucleation theory employ combinations of thermodynamic and kinetic descriptions. These models are also able to predict similar experimental data reasonably well, albeit with some adjustable parameters. At this point, which of these two approaches provides a more accurate description of the mechanism of nucleation needs to be determined. A sure test of the validity of one approach over the other lies in their predictions of the dependence of R^* on ϕ. According to the present model, R^* is defined kinetically and passes through a minimum upon increasing ϕ. Classical theories, on the other hand, define R^* from thermodynamics alone, as the size at which the free energy change associated with crystal formation is a maximum. R^*, therefore, decreases monotonically upon increasing ϕ. Unfortunately, experiments measuring R^* beyond $\phi = 0.56$, where the present model predicts the minimum, have not yet been performed.

VI. CONCLUSIONS

The kinetics of crystallization in HS suspensions is captured well by the model presented here. Upon increasing the particle volume fraction in suspension above the solubility point, an increase in the thermodynamic driving force for crystallization enhances the nucleation rate. At very high volume fractions, however, the concentration gradient between the surface of a crystal nucleus and the bulk suspension diminishes. The aggregation of particles onto the crystal surface, being driven by gradient diffusion, also diminishes, reducing the nucleation rate. As a result of these competing influences, a maximum in the nucleation rate is predicted at an intermediate volume fraction of about 0.56. Model predictions of nucleation rates and growth velocities show excellent agreement with experimental observations.

To make quantitative comparisons with data, the model introduces two adjustable parameters to characterize the structure of the surface of a growing crystal. We show that these parameters correspond to the curvature and the volume fraction dependence of the solid/fluid surface tension, which are typically used as adjustable parameters in classical nucleation theories. Our model, however, differs from the classical approach by building a completely kinetic description of the

nucleation mechanism. The two approaches make very different predictions for the variation of the critical cluster size with volume fraction. While the present model predicts a minimum, the classical approach predicts a monotonic decrease in the critical cluster size with increasing volume fraction. Measurements of the critical cluster sizes at different volume fractions would thus provide for an experimental validation of the two approaches, clarifying the mechanism of crystal nucleation in colloidal suspensions.

ACKNOWLEDGMENT

The authors acknowledge support from the U.S. DOE via the University of Illinois at Urbana-Champaign, Frederick Seitz Materials Research Laboratory, Grant No. DEFG02-96ER45439.

[1] P. V. Braun and P. Wiltzius, Nature (London) **402**, 603 (1999).
[2] A. McPherson, *Preparation and Analysis of Protein Crystals* (Kreiger, Malabar, FL, 1982).
[3] B. J. Alder and T. E. Wainwright, J. Chem. Phys. **27**, 1208 (1957).
[4] S. Hachisu and Y. Kobayashi, J. Colloid Interface Sci. **46**, 470 (1974).
[5] P. N. Pusey and W. van Megen, Phys. Rev. Lett. **59**, 2083 (1987).
[6] M. Muschol and F. Rosenberger, J. Chem. Phys. **107**, 1953 (1997).
[7] D. F. Rosenbaum and C. F. Zukoski, J. Cryst. Growth **169**, 752 (1996).
[8] D. F. Rosenbaum, P. C. Zamora, and C. F. Zukoski, Phys. Rev. Lett. **76**, 150 (1996).
[9] S. M. Ilett, A. Orrock, W. C. K. Poon, and P. N. Pusey, Phys. Rev. E **51**, 1344 (1995).
[10] H. N. W. Lekkerkerker, W. C. K. Poon, P. N. Pusey, A. Stroobants, and P. B. Warren, Europhys. Lett. **20**, 559 (1992).
[11] W. B. Russel, Phase Transitions **21**, 127 (1990).
[12] B. J. Ackerson and K. Schatzel, Phys. Rev. E **52**, 6448 (1995).
[13] O. Galkin and P. G. Vekilov, J. Phys. Chem. B **103**, 10 965 (1999).
[14] P. R. ten Wolde and D. Frenkel, Science **277**, 1975 (1997).
[15] T. Palberg, J. Phys.: Condens. Matter **11**, R323 (1999).
[16] K. Schatzel and B. J. Ackerson, Phys. Rev. E **48**, 3766 (1993).
[17] N. M. Dixit, A. M. Kulkarni, and C. F. Zukoski, Colloids Surf., A **190**, 47 (2001).
[18] J. K. G. Dhont, C. Smits, and H. N. W. Lekkerkerker, J. Colloid Interface Sci. **152**, 386 (1992).
[19] J. Zhu, M. Li, R. Rogers, W. Meyer, R. H. Ottewill, W. B. Russel, and P. M. Chaikin, Nature (London) **387**, 883 (1997).
[20] D. Z. Cheng, W. B. Russel, and P. M. Chaikin, Nature (London) **401**, 893 (1999).
[21] D. J. W. Aastuen, N. A. Clark, L. K. Cotter, and B. J. Ackerson, Phys. Rev. Lett. **57**, 1733 (1986).
[22] Y. He, B. J. Ackerson, W. van Megen, S. M. Underwood, and K. Schatzel, Phys. Rev. E **54**, 5286 (1996).
[23] K. E. Davis and W. B. Russel, Ceram. Trans. **1B**, 693 (1988).
[24] J. L. Harland and W. van Megen, Phys. Rev. E **55**, 3054 (1997).
[25] N. M. Dixit and C. F. Zukoski, J. Colloid Interface Sci. **228**, 359 (2000).
[26] G. Narasimhan and E. Ruckenstein, J. Colloid Interface Sci. **128**, 549 (1989).
[27] D. A. McQuarrie, *Statistical Mechanics* (Harper and Row, New York, 1976).
[28] N. F. Carnahan and K. E. Starling, J. Chem. Phys. **51**, 635 (1969).
[29] K. R. Hall, J. Chem. Phys. **57**, 2252 (1972).
[30] B. Nowakowski and E. Ruckenstein, J. Colloid Interface Sci. **139**, 500 (1990).
[31] U. Gasser, E. R. Weeks, A. Schofield, P. N. Pusey, and D. A. Weitz, Science **292**, 258 (2001).
[32] W. B. Russel, D. A. Saville, and W. R. Schowalter, *Colloidal Dispersions* (Cambridge University Press, Cambridge, 1989).
[33] D. W. Marr and A. P. Gast, Phys. Rev. E **47**, 1212 (1993).
[34] M. D. Rintoul and S. Torquato, Phys. Rev. E **58**, 532 (1998).
[35] J. Chang and S. I. Sandler, Mol. Phys. **81**, 735 (1994).
[36] D. I. Zhukhovitskii, J. Chem. Phys. **101**, 5076 (1994).
[37] R. C. Tolman, J. Chem. Phys. **17**, 333 (1949).
[38] J. Schmelzer, J. Chem. Soc., Faraday Trans. 1 **82**, 1421 (1986).
[39] V. I. Kalikmanov, Phys. Rev. E **55**, 3068 (1997).
[40] P. R. ten Wolde and D. Frenkel, J. Chem. Phys. **109**, 9901 (1998).
[41] V. Talanquer and D. W. Oxtoby, J. Chem. Phys. **99**, 2865 (1995).
[42] J. Shmelzer and R. Mahnke, J. Chem. Soc., Faraday Trans. 1 **82**, 1413 (1986).
[43] M. Iwamatsu, J. Phys.: Condens. Matter **6**, L173 (1994).
[44] J. Israelachvili, *Intermolecular and Surface Forces* (Academic, London, 1992).
[45] O. Sinanoglu, Chem. Phys. Lett. **81**, 188 (1981).
[46] S. Auer and D. Frenkel, Nature (London) **409**, 1020 (2001).
[47] W. B. Russel, P. M. Chaikin, J. Zhu, W. V. Meyer, and R. Rogers, Langmuir **13**, 3871 (1997).